Appendix A. The selection of parameters in the transportation scenario

The travel demand pattern faced by SAEV systems can be inspired by the demands faced by urban Taxis. Therefore, we collected a Taxi GPS dataset with 275254 data for about 2000 Taxis serving in Beijing on August 2, 2020. As shown in Table A.1, it records the GPS location of each Taxi every few minutes on this day. The last three columns record the status of the vehicle, where passenger equals 1 indicates the presence of a passenger. After pre-processing, the dataset was cleaned to 227,296 data points. Then, we divided the study area into a number of grids with an accuracy of 500 m and mapped each GPS data point to the corresponding grid, as shown in Figure A.1. Furthermore, based on the state of the car and the temporal order of the data points, travel data can be generated with the grid as the origin and destination. These data are then averaged to the node-based traffic map to form the travel demand pattern, represented by the colors in Figure 4. The results in Figure 4 are calculated using data from 2000 Taxis for one day. We can randomly select data from some of these Taxis over a period of time and use the same method to calculate them. For example, choosing the data points of Taxis with ID from 1 to 200 from 9:00 to 10:00 to be calculated so that we can get a list of travel demand patterns faced by a Taxi system containing 200 vehicles during that time period. We consider these results, calculated based on the Taxi GPS dataset, as the travel demand the SAEV system must withstand.

Table A.1: Part of Taxi GPS dataset in Beijing

Vehicle ID	Time	Longitude	Latitude	Angle	Velocity	Passenger
1	23:23:18	116.2903334	39.94450624	0	51	1
1	23:46:42	116.438982	39.93245931	4	72	1
2	00:12:19	116.4375872	39.91124829	6	11	1
2	00:13:32	116.3408096	39.88738176	336	14.82	0

Since there are no actual SAEVs, we can only assume vehicle parameters based on those EV types that already exist. The Tesla Model S was chosen because it is one of the most advanced electric vehicles, at a relatively high level of autonomous driving. The vehicle parameters in our case are given in Table A.2. Here the speed is assumed to be a fixed

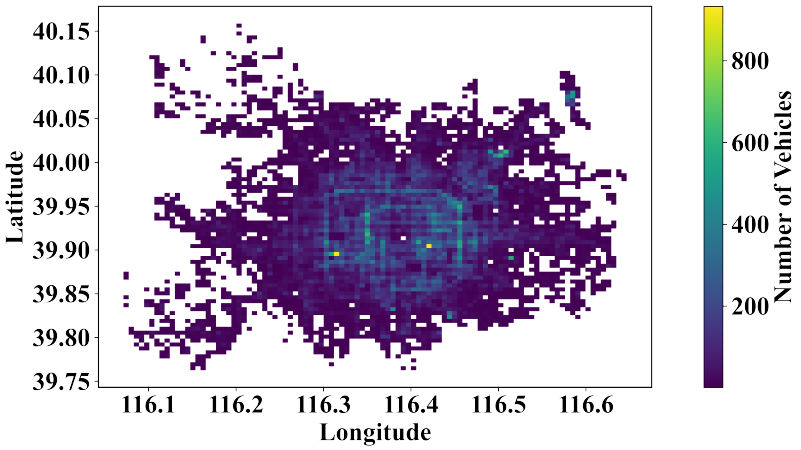

Figure A.1: Counting of Taxi GPS Trajectory Points

value, which is based on the average of our Taxi GPS dataset.

Table A.2: Parameters of SAEV

Parameter	Battery Capacity	Charging rate	Discharging rate(V2G)	Consumption rate	Velocity
Value	100Kwh	2Kw(220V) 50Kw(440V)	2Kw(220V) 50Kw(440V)	0.162Kwh/Km	40Km/h

Appendix B. The selection of parameters in the power grid scenario

Here, we try to build a grid system on some reasonable assumptions. First, since the traffic nodes represent a region, it is assumed that each traffic node has charging stations with the ability to power SAEVs. Secondly, to simplify the model, the transmission process between power plants and charging stations in the same region is ignored, so the power plants are averaged to the charging station nodes according to the distance and region, as shown in Figure B.2. The generation capacity of each node is the sum of the generation capacity of the subordinate power plants, which is listed in Table B.4. About the ramp rate, the assumption is proposed that the larger the unit is, the higher the ramp rate is. Since

some generators are aggregated, the setting is dependent on the maximum capacity of the subordinated power plant. Accordingly, the ramp rate is set as in Table B.4.

Besides, the target grid is regarded as an isolated and closed system because the overall generation of the power plants we consider (all plants we can find in Beijing) is higher than the overall consumption of the study area, as shown in Table B.3 and Table A.1. Another assumption is that our target grid only considers the transmission phase, not the distribution phase, because of its high computational cost and lack of data. Figure B.3 shows the grid structure of Beijing's 110 Kv/220 Kv transmission line, which roughly presents a form of a polygon. Therefore, a similar transmission line topology is chosen as the structure of the grid, as shown in Figure 5.

In Beijing, 220 Kv transmission lines are the main lines for grid transmission. The reactance of such lines was measured to be 0.3296 ohm/Km/phase. Three-phase AC is used as a form of transmission in Beijing, and it is assumed that the distance of each line is the Euclidean distance between two nodes, so the reactance of each line can be calculated, as shown in Table A.2. The limit of voltage angle difference is set to $\pm 30°$. Typically, the power flow capacity of a 220 Kv line is about 300 Mw. However, in our model, the lines between nodes are a collection of several or more lines, so we assume that the capacity of a line is a multiple of 300 Mw. We tested the consumption demand in Table A.1 on the basis of the grid that has been established so far and calculated the possible flows for each transmission line, as shown in Table A.2. Suitable transmission caps were then selected for these lines.

We distinguished the peak and low time periods of electricity consumption in the target area based on the electricity prices in Beijing, as shown in Figure B.4, and used the electricity consumption given in Table A.1 as the value for the peak period since it almost reaches the maximum generation capacity of our grid system. The electricity consumption during normal hours and low periods is 70 and 40 percent of the peak period, respectively.

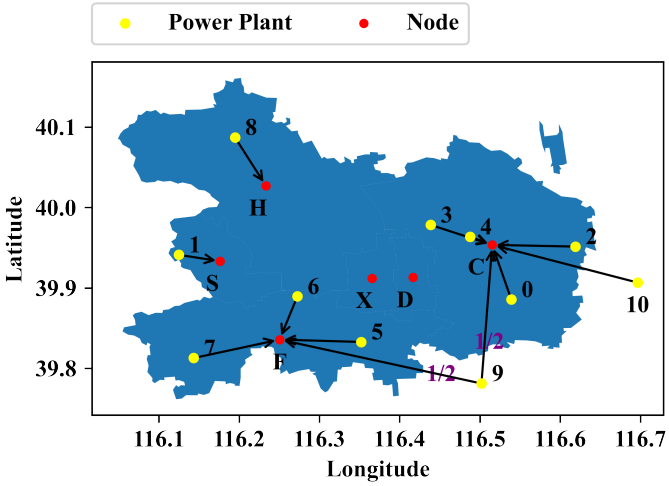

Figure B.2: Aggregation of power plants

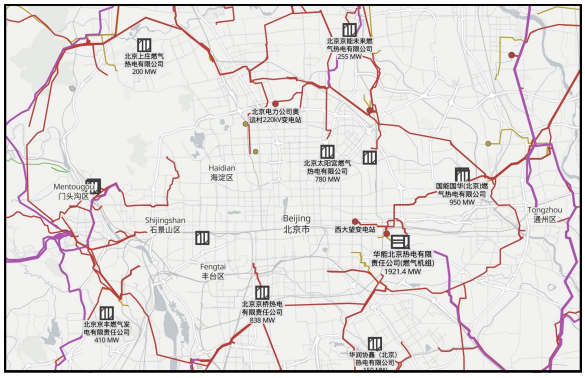

Figure B.3: The power grid in Beijing

Table B.3: Information about power plants in Beijing (HNBJ: Huaneng Beijing Gas Power Plant; DTGJ: Datang Gaojing Gas Power Plant; GAT: Gao'antun Gas Power Plant; SP: Sun Palace Gas Power Plant; ZD: Zhengdong Group South Gas Power Plant; CQ: Beijing Southwestern Caoqiao Gas Power Plant; ZCZ: Zhengchangzhuang Gas Power Plant; JF: Jingfeng Gas Power Plant; SZ: Beijing North Haidian District Shangzhuang Gas Power Plant; CRC: CRC GCL Gas Power Plant; HDBR: Beijing Huadian Beiran Tongzhou Yunhe Central District Distributed EnergyStation)

Number	0	1	2	3	4	5
Power Plant	HNBJ	DTGJ	GAT	SP	ZD	CQ
Generation Capacity (Mw)	998	1430	845	700	112.4	840
Generation Capacity (Mkwh/year)	8742.48	12526.80	7402.20	6132.00	984.624	7358.4
Number	6	7	8	9	10	
Power Plant	ZCZ	JF	SZ	CRC	HDBR	Overall
Generation Capacity (Mw)	508	390	266	150	255	6494.4
Generation Capacity (Mkwh/year)	4450.08	3416.4	2330.16	1314.00	2233.80	56890.944

Appendix C. The calculation of capacity factors of the renewable energy generation

Generally, renewable energy resources include wind power and solar-PV power, whose generation is highly related to the climate data, such as solar irradiance or surface-downwelling shortwave (i.e., wavelength interval 0.2–4.0 μm) radiation (rsds), and wind speed, etc. The method to calculate the capacity factor with wind speed is presented as follows. Hourly wind speed data from July 20th to August 10th in 5 years (2018-2022) are averaged to 22 hourly wind speed profiles. We further average these data to one typical profile. Based on

Table B.4: Generation capacity and ramp rate of each node

Node number	X-1	D-2	C-3	F-4	S-5	H-6
Generation Capacity (Mw)	0	0	1813	2985.4	1430	266
Ramp rate (Per min)	0	0	0.11	0.11	0.12	0.04

Table B.5: Electricity consumption in different regions

District	Dong Cheng	Xi Cheng	Chao Yang	Feng Tai	Shi Jing Shan	Hai Dian	Overall
Consumption (Mkwh)	4477.32	5249.15	18625.64	8944.14	2265.23	14969.55	54531.03
Consumption (Mw)	511.11	599.22	2126.21	1032.03	258.59	1708.85	6236.01

the hourly wind speed V, turbine-generated electric power capacity factor at node i, CF_i is calculated by a standard power curve, described as follows:

$$CF_i = \begin{cases} 0, & if \quad V < V_l \quad or \quad V > V_0 \\ \dfrac{V^3 - V_l^3}{V_R^3 - V_l^3}, & if \quad V_l \leq V < V_R \\ 1, & if \quad V_R \leq V < V_0 \end{cases} \tag{C.1}$$

where V_l, V_R and V_0 are the cut-in, rated, and cut-out velocity of a wind turbine, respectively. The wind power capacity factor is calculated at the grid cell level (defined in the climate projection model), assuming a unique turbine model for all grid cells. Typically, there are two managed forms of turbines, one centralized and one distributed. In our target area, where the residential density is high, centralized generation is not possible, so distributed generation is assumed. Due to the low wind speed, a domestic type is the best choice for the turbine model in our case. According to the available technologies, we set the V_l, V_R and V_0, respectively, as 1.5m/s, 9m/s, and 50m/s. Then, an hourly capacity factor profile is calculated as shown in Figure C.5 (left).

Using the same method as we did in the wind power part, a typical profile of surface

Table B.6: Parameters of transmission lines

Line number	1	2	3	4	5	6
Reactance (ohm)	3.9552	9.8880	16.8096	25.7087	12.8544	15.8208
Power flow (Mw)	599.22	451.92	658.41	1294.96	2466.37	765.13
Capacity (Mw)	900	600	900	1500	2700	1200

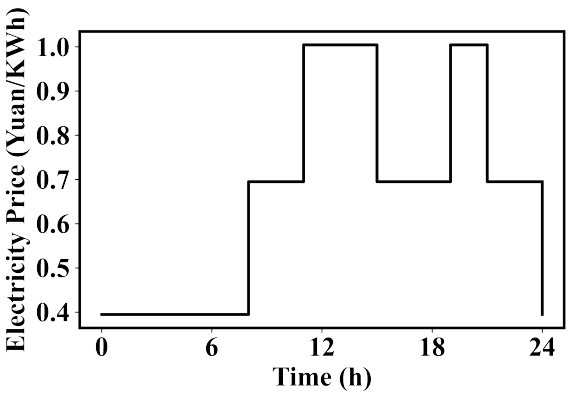

Figure B.4: The electricity price evolution of Beijing

temperature and irradiance in Beijing is generated. The equation to calculate the capacity factor is expressed as:

$$CF_i = [1 + \gamma \left(T_{cell} - T^0\right)] \frac{rsds}{rsds^0} \tag{C.2}$$

In which, parameter γ is set at $-0.005°C^{-1}$, reflecting the impact of typical temperature efficiency of monocrystalline silicon solar panels. T^0 and $rsds^0$ are, respectively, the temperature and solar irradiance under the standard test conditions for which the nominal capacity of a PV device is determined as its measured power ($rsds^0 = 1000\ Wm^{-2}$, $T^0 = 25°C$). As for the PV cell temperature, T_{cell} is determined by Eq.(C.3).

$$T_{cell} = c_1 + c_2 tas + c_3 rsds + c_4 V \tag{C.3}$$

Where, $c_1 = 4.3°C$, $c_2 = 0.943$, $c_3 = 0.028°Cm^2W^{-1}$ and $c_4 = -1.528°Csm^{-1}$. tas is the surface air temperature and V denotes the wind speed. Finally, the calculated results of

capacity factor are shown in Figure C.5 (right), which indicate the high potential of solar-PV power generation in Beijing.

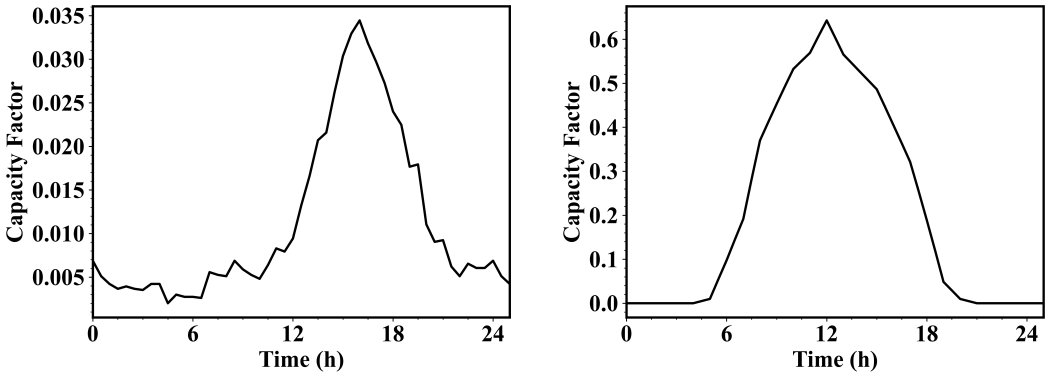

Figure C.5: Capacity factor of Wind power (left) and solar-PV power (right) generation

Appendix D. The selection of the prediction horizon (PH) and control horizon (CH)

The CH determines the number of subproblems. Generally, when the schedule horizon (SH) is not high, CH is always set to 1, so that the computational results of each step are obtained under the subproblem with the new information added while the number is not excessive.

The value of PH determines the size of the subproblem, and the smaller it is, the lower the size. However, the PH must be larger than the maximum time distance $\tau_{i,j_{max}}$. Otherwise, the vehicle rebalances between these two nodes would be neglected. The reason is that the vehicles in one of the nodes cannot reach the other one and carry the passengers waiting there in the considered PH. Therefore, they cannot contribute to the objective function of the subproblem, so these possibilities are rejected. Based on the scale of the scenario we are considering, we set the time resolution to 30 min, so the maximum time distance is calculated to 2. As a result, the PH must be larger than 2.

To further determine the value of PH, we calculated the average waiting time (AWT, defined in section 6.2) of the SAEV system with PH of 3, 4, 5, and 6 in the same scenario,

respectively. The scenario here is similar to the one in the charging rate analysis in section 6.2 while the charging rate is fixed at 0.25. The results are shown in Figure D.6. Larger PH translates into lower peak waiting times, although the change is minimal after 4. Therefore, setting PH to 4 is a reasonable choice in terms of calculation complexity and stability of calculation results.

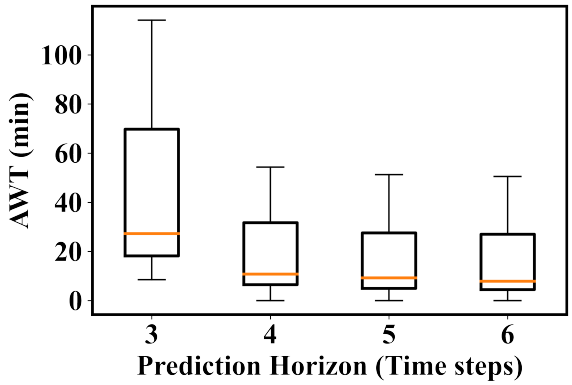

Figure D.6: The average waiting time (AWT) in different prediction horizon (PH).